LAWRENCE
LIVERMORE
NATIONAL
LABORATORY

UCRL-JRNL-223884

Influence of Dust Composition on Cloud Droplet Formation

J. T. Kelly, C. C. Chuang, A. S. Wexler

August 22, 2006

Atmospheric Environment

Updated October 14, 2003

8/21/2006

Title: Influence of Dust Composition on Cloud Droplet Formation

Authors: James T. Kelly[1,4,*], Catherine C. Chuang[4], and Anthony S. Wexler[1,2,3]

Affiliations:

[1]Department of Mechanical and Aeronautical Engineering

[2]Department of Civil and Environmental Engineering

[3]Department of Land, Air and Water Resources

University of California, Davis, CA, USA

[4]Energy & Environment Directorate

Lawrence Livermore National Laboratory

Livermore, CA, USA

To be submitted to Atmospheric Environment

[*]**Corresponding Author:**

James T. Kelly

Lawrence Livermore National Laboratory

7000 East Ave, L-103

Livermore, CA 94550

E-mail: jimkelly@ucdavis.edu

Phone: 925-423-0358

Fax: 925-423-4908

Abstract

Previous studies suggest that interactions between dust particles and clouds are significant; yet the conditions where dust particles can serve as cloud condensation nuclei (CCN) are uncertain. Since major dust components are insoluble, the CCN activity of dust strongly depends on the presence of minor components. However, many minor components measured in dust particles are overlooked in cloud modeling studies. Some of these compounds are believed to be products of heterogeneous reactions involving carbonates. In this study, we calculate Kohler curves (modified for slightly soluble substances) for dust particles containing small amounts of K^+, Mg^{2+}, or Ca^{2+} compounds to estimate the conditions where reacted and unreacted dust can activate. We also use an adiabatic parcel model to evaluate the influence of dust particles on cloud properties via water competition. Based on their bulk solubilities, K^+ compounds, $MgSO_4 \cdot 7H_2O$, $Mg(NO_3)_2 \cdot 6H_2O$, and $Ca(NO_3)_2 \cdot 4H_2O$ are classified as highly soluble substances, which enable activation of fine dust. Slightly soluble gypsum and $MgSO_3 \cdot 6H_2O$, which may form via heterogeneous reactions involving carbonates, enable activation of particles with diameters between about 0.6 and 2 μm under some conditions. Dust particles > 2 μm often activate regardless of their composition. Only under very specialized conditions does the addition of a dust distribution into a rising parcel containing fine $(NH_4)_2SO_4$ particles significantly reduce the total number of activated particles via water competition. Effects of dust on cloud saturation and droplet number via water competition are generally smaller than those reported previously for sea salt. Large numbers of fine dust CCN can significantly enhance the number of activated particles under certain conditions. Improved representations of dust mineralogy and reactions in global aerosol models could improve predictions of the effects of aerosol on climate.

1. Introduction

Large quantities of dust particles are entrained into the atmosphere in arid and semi-arid environments. Interactions between dust and clouds may be an important pathway for aerosol to influence climate. Under some conditions, dust particles can suppress precipitation by providing large concentrations of cloud condensation nuclei (CCN) that lead to the formation of clouds dominated by small droplets with low coalescence efficiencies (Rosenfeld et al., 2001). Conversely, dust particles may enhance precipitation formation in some continental environments by providing giant CCN that form large droplets with high collection efficiencies (e.g., Yin et al., 2002). Dust that is acidified through cloud processing may be an important source of bioavailable iron to oceans (Meskhidze et al., 2005), and dust particles that act as CCN have reduced atmospheric lifetimes (Fan et al., 2004). Also, water uptake by coarse dust particles could reduce cloud saturation and inhibit activation of more numerous fine particles.

Despite the importance of dust particles as CCN, the conditions for which dust can activate into cloud droplets are unclear. When first emitted, dust particles are often composed of insoluble or low-solubility components. In modeling studies, the assumption is sometimes made that cloud droplets cannot nucleate on these particles (Wurzler et al., 2000; Yin et al., 2002). However, several laboratory studies report multilayer water coverage on insoluble dust and calcium carbonate at relative humidities (RHs) less than 100% (Chiarello et al., 1993; Gustafsson et al., 2005; Seisel et al., 2005). These measurements suggest that freshly emitted dust particles can serve as CCN under some conditions.

During transport, $CaCO_3$ in dust can react with gases such as HNO_3 and SO_2 to form components that may enhance dust's ability to serve as CCN. The main product of the HNO_3 reaction is calcium nitrate, which deliquesces at low RH and greatly enhances dust

hygroscopicity (Laskin et al., 2005). In the case of the SO_2 reaction with $CaCO_3$, calcium sulfite appears to form, and the sulfite can be oxidized to sulfate by gas-phase ozone (Usher et al., 2002). Since the solubility of calcium sulfite is similar to that of $CaCO_3$, the SO_2 reaction may not enhance the hygroscopicity of dust initially. If gypsum ($CaSO_4 \cdot 2H_2O$) forms subsequently through sulfite oxidation, the resulting particles could be more efficient CCN than the original $CaCO_3$-containing dust. However, the significance of this enhancement is unclear because gypsum is only slightly soluble (Linke and Seidell, 1965; Laaksonen et al., 1998). For dust particles without carbonates, condensation of H_2SO_4 could lead to a highly soluble form of sulfate, such as $(NH_4)_2SO_4$, coating the surface of the dust. The potential of reacted dust particles to serve as CCN is likely to depend on the particular reaction products for some atmospheric conditions. Yet studies on the activation of reacted dust treat the particles as having an insoluble core with a highly soluble sulfate coating and do not consider slightly soluble or non-sulfate products (Fan et al., 2005).

In addition to the dust components just mentioned, numerous other compounds can influence the nucleation of cloud droplets on dust. Ro et al. (2005) reported components such as $MgCO_3$, $MgSO_4$, K_2CO_3, KNO_3, and K_2SO_4 in single-particle measurements of Asian dust sampled in Korea. The nitrate and sulfate components may have formed during transport via heterogeneous reactions with carbonates. Other studies report the presence of halite (NaCl) in dust aerosols (e.g., Andronova et al., 1993; Gill, 1996). Okada and Kai (2004) detected halite that was believed to originate from salt flats in about 10% of dust particles collected at Qira in the Taklamakan Desert. Trace amounts of soluble material in dust particles can drastically reduce the saturation required for activation (Dusek et al., 2006), and a recent study by Roberts et al. (2006) indicates that chemical composition may have an important influence on the

activation of long-range transported Asian dust. Therefore the numerous minor components present in dust at emission and acquired during transport may strongly influence dust's ability to serve as CCN under some conditions.

The primary goals of this study are to evaluate how heterogeneous reactions with carbonates influence dust activation and to investigate the effects of dust on cloud properties via water competition. Improved understanding of these issues will improve treatments of dust-cloud interactions in global aerosol models and predictions of aerosol effects on climate. First, conditions where dust particles can act as CCN are estimated from Kohler curves for dust containing insoluble, slightly soluble, and highly soluble components, as well as their mixtures. Next, the influence of dust on cloud saturation and number of activated particles is investigated by introducing dust distributions into an adiabatic parcel model containing a fine $(NH_4)_2SO_4$ distribution.

2. Approach

2.1 Dust Composition

The components of dust particles considered here that may dissolve in water are listed in Table 1 with their deliquescence relative humidities (DRHs) (where available) and solubilities. While the stable hydrates are generally indicated, the actual solid phases in dust particles are unclear in some cases. The components treated as slightly soluble are $CaCO_3$, $MgCO_3$, $MgCO_3 \cdot 3H_2O$, $CaSO_3 \cdot 0.5H_2O$, $MgSO_3 \cdot 6H_2O$, and $CaSO_4 \cdot 2H_2O$; the remaining compounds in Table 1 are treated as highly soluble (i.e., deliquescent). Quartz is chosen to represent the insoluble portion of dust particles. We do not consider insoluble smectite clays that swell by acquiring water with increasing relative humidity (Hensen and Smit, 2002; Frinak et al., 2005)

The carbonate content of dust appears to be highest in the coarse size fraction (Pye, 1987; Usher et al., 2003) and varies considerably with source region. For instance, Wang et al. (2005) reported that the carbonate content of soils in northern China decreases systematically from west to east from 11.8% to 0.3%. Alpert and Ganor (2001) reported high carbonate content (29% $CaCO_3$, 26% $CaMg(CO_3)_2$) for non-clay minerals sampled in Israel that appeared to originate from Algeria, Libya, and Israel. Laskin et al. (2005) found little carbonate in Saharan and inland Saudi Arabian soil, but significant carbonate in soil from coastal Saudi Arabia and China. Given the regional differences in carbonate content, we consider a range of compositions.

2.2 Equilibrium (Kohler) Theory

Curves based on the modified Kohler equation (Shulman et al., 1996; Laaksonen et al., 1998) illustrate the water saturation required to activate particles containing slightly soluble components (SSCs). According to modified Kohler theory, the saturation ratio of water (S_w) for a particle containing an insoluble, slightly soluble, and highly soluble component is expressed as

$$S_w \approx 1 + \frac{4M_w\sigma_w}{RT\rho_w D} - \frac{6M_w\nu_{HSC}n_{HSC}}{\pi\rho_w(D^3 - D_{core}^3)} - \gamma_{SSC}, \quad (1)$$

$$\gamma_{SSC} = \frac{M_w\nu_{SSC}\Gamma_{SSC}}{M_{SSC}} \text{ for } n_w < n_w^0, \quad (2)$$

$$\gamma_{SSC} = \frac{M_w\nu_{SSC}\Gamma_{SSC}n_w^0}{M_{SSC}n_w} \text{ for } n_w > n_w^0, \quad (3)$$

where D is the particle diameter, D_{core} is the diameter of the undissolved particle core (quartz plus undissolved SSC), M_w is the molar mass of water, σ_w is the surface tension of water, R is the gas constant, T is the temperature, ρ_w is the density of water, n_{HSC} is the number of moles of the highly soluble component (HSC), ν_{HSC} is the number of moles of ions formed from the

dissociation of one mole of the parent HSC, Γ_{SSC} is the solubility of the SSC (kg-SSC/kg-H_2O), M_{SSC} is the molar mass of the SSC, n_w^0 is the number of moles of water needed to completely dissolve the SSC, and n_w is the number of moles of water in the particle solution. Droplets and particle cores are assumed to be spherical in our calculations.

The third term on the right side of (1) describes the reduction in the saturation ratio by highly soluble compounds, and the fourth describes that due to slightly soluble ones. The absolute effect of the HSC on the saturation ratio increases with decreasing particle diameter as this substance concentrates in the particle solution. The effect of the SSC on the saturation ratio is constant because this substance precipitates to maintain the solubility concentration as particle water decreases. The HSC and SSC are assumed not to react with each other in the derivation of (1)–(3) (Laaksonen et al., 1998); however, the influence of the HSC on the solubility of the SSC can be taken into account as necessary when solubility data for the mixed solution are available. Curves based on (1)–(3) are given in Section 3.1 for representative dust compositions and are used to estimate conditions for which dust particles can activate into cloud droplets.

2.3 Kinetic Considerations

Ghan et al. (1998) reported that the addition of a sea-salt distribution into a rising parcel containing an $(NH_4)_2SO_4$ distribution can increase or decrease the overall cloud droplet number depending on the atmospheric conditions. Similarly, coarse dust particles may enhance the cloud droplet number by providing CCN or decrease the droplet number by reducing the cloud saturation and inhibiting activation of numerous fine particles. Here we use an adiabatic parcel model with detailed microphysics to investigate the influence of dust distributions externally mixed with a fine $(NH_4)_2SO_4$ distribution on parcel saturation and the number of activated particles.

The adiabatic model is based on the standard prognostic equations for conservation of heat and moisture in a one-dimensional parcel rising with constant velocity. The equations are not given here because they are readily available elsewhere (e.g., Seinfeld and Pandis, 1998, Chapter 15). Condensational particle growth is calculated similar to Majeed and Wexler (2001); however, the saturation ratio of water is determined in the transport equation according to (1)–(3) to account for slightly soluble substances. Since our focus is on the formation of cloud droplets and collision efficiencies are small in the early stages of cloud development, droplet collisions are not considered in the model. Simulations are initialized with T = 280 K and pressure = 1000 mbar. Constant updraft velocities range from 0.05 to 1 m/s. The accommodation coefficient for water vapor is 1, the thermal accommodation coefficient is 0.96, the vapor jump length is 1.096×10^{-5} cm, and the thermal jump length is 2.16×10^{-5} cm. The $(NH_4)_2SO_4$ aerosol is represented by a lognormal number distribution with a geometric mean diameter (D_g) of 0.16 μm and geometric SD (σ_g) of 1.4. These conditions (simulation parameters and $(NH_4)_2SO_4$ distribution) match those of Ghan et al. (1998) and allow water competition due to dust to be compared with previous results for sea salt. However, we initially equilibrate aerosol at an RH of 97% rather than 100% (Ghan et al., 1998) to account for kinetic limitations near the cloud base (Nenes et al., 2001; Phinney et al., 2003). Coarse dust is represented by a lognormal distribution with σ_g = 2.0 and D_g = 1.5 or 2.2 μm, which is suitable for long-range transported dust (e.g., Patterson and Gillette, 1977; McTainsh et al., 1997; Singer et al., 2004). A case in which dust is represented by a trimodal distribution is also considered: D_{g1} = 0.2 μm, D_{g2} = 0.8 μm, D_{g3} = 2.0 μm based on Levin et al. (2005), $\sigma_{g1} = \sigma_{g2} = \sigma_{g3}$ = 2.0. A giant dust mode (> 5 μm) is not considered because of the short atmospheric lifetime and low concentration of these particles. One hundred bins evenly spaced in log diameter are used to represent each distribution.

Calculation of the water vapor pressure according to (1)–(3) assumes that particle water is saturated with the slightly soluble component until this substance fully dissolves. However, the solution will be subsaturated if the dissolution rate of the SSC is slow compared to the condensation rate of water. The following ratio can be used to determine if the solution is subsaturated due to kinetic limitations:

$$Ratio = \left(\frac{dm}{dt}\right)_{water} \Gamma_{SSC} \Big/ \left(\frac{dm}{dt}\right)_{SSC}, \qquad (4)$$

where $\left(\frac{dm}{dt}\right)_j$ is the rate of change of mass of component *j* in the particle solution. The solubility factor in the numerator normalizes the expression so that Ratio < 1 indicates a saturated solution and Ratio > 1 indicates a subsaturated (kinetically limited) solution.

Calculation of the ratio in (4) is difficult for several reasons. The dissolution rates required to determine $\left(\frac{dm}{dt}\right)_{SSC}$ are complex functions of solution properties and are not available for some substances. The dissolution measurements that are available are for bulk experiments that may not represent conditions in a growing particle. Also, calculation of (4) requires information on the surface area of the dissolving substance, which is difficult to specify accurately. Here we set the SSC concentration to the solubility (i.e., equilibrium) value in growth calculations when solid-phase SSC is present in the droplet core. We consider estimates of (4) in situations where dissolution kinetics could be important.

3. Results and discussion

3.1 Kohler Curves for Dust Particles

Kohler curves illustrating the saturation ratio (ratio of the water vapor pressure above a curved solution droplet to that above a flat pure water surface) are given in Figure 1 for dust particles (0.8 μm dry diameter) containing an insoluble quartz (SiO_2) core coated with slightly soluble calcium components. The curves have attributes of the Kelvin curve for pure water. Since no highly soluble substances are present in the particles, the third term on the right side of (1) is zero and (1) reduces to the Kelvin equation modified by a constant factor ($-\gamma_{SSC}$). The constant factor is determined by the solubility of the SSC and shifts the curves to lower saturation ratios than those of the traditional Kelvin curve for pure water. Since the solubilities of $CaCO_3$ and $CaSO_3 \cdot 0.5H_2O$ are small (Table 1), the curve for these components is very close to that of pure water (Figure 1). For cloud supersaturations of 0.2%, $CaCO_3$ and $CaSO_3 \cdot 0.5H_2O$ particles will activate if they have dry sizes greater than about 1 μm.

For quartz particles coated with gypsum, saturation ratios are reduced by $\gamma_{SSC} = 5.4 \times 10^{-4}$ compared to pure water for diameters where solid-phase gypsum is present in the particle core. Following the gypsum-SiO_2 curve in Figure 1 from left to right, notice that the saturation ratios are equal to those of pure water minus $\gamma_{SSC} = 5.4 \times 10^{-4}$ until the diameters are reached where the different percentages of gypsum fully dissolve and the saturation ratios abruptly increase with diameter. For cloud supersaturations of 0.2%, gypsum-coated particles with diameters greater than about 0.8 μm will activate. For some lower supersaturations, particles coated with gypsum could initially activate, but then deactivate when they grow beyond the size where all gypsum dissolves and the saturation ratio increases with further growth (Figure 1).

Kohler curves for particles coated with slightly soluble magnesium compounds are shown in Figure 2. Similar to $CaCO_3$ and $CaSO_3 \cdot 0.5H_2O$, the solubility of $MgCO_3$ (magnesite)

is low and saturation ratios for $MgCO_3$-coated particles are very close to those for a pure water particle. For particles coated with $MgCO_3 \cdot 3H_2O$, the curves are similar to those just discussed for gypsum because the solubilities of these compounds are similar. Although the stable form of magnesium carbonate is the trihydrate at 298 K (e.g., Kline, 1929), the anhydrous form is also common in nature. Various forms of magnesium carbonate ($MgCO_3$, $MgCO_3 \cdot 3H_2O$, $CaMg(CO_3)_2$, etc.) are likely to be present in small amounts in dust particles.

The solubility of $MgSO_3 \cdot 6H_2O$ is the highest of the SSCs considered and corresponds to a reduction in saturation ratio of $\gamma_{SSC} = 1.8 \times 10^{-3}$ compared with pure water particles. For supersaturations of 0.2%, $MgSO_3 \cdot 6H_2O$-coated particles with diameters greater than about 0.55 μm will activate. For lower saturation ratios, some $MgSO_3 \cdot 6H_2O$-coated particles could initially activate and then deactivate after all $MgSO_3 \cdot 6H_2O$ dissolves and the saturation ratio begins to increase with diameter (Figure 2). Magnesium sulfite could form in dust via reactions between SO_2 and magnesium carbonates; e.g.,

$$MgCO_3(s) + SO_2(g) + nH_2O \leftrightarrow MgSO_3 \cdot nH_2O(s) + CO_2(g), \qquad \text{(R1)}$$

where n is the hydration number. In Figure 3, equilibrium concentrations of SO_2 for (R1) are shown. The equilibrium calculations were made according to Kelly and Wexler (2005). For atmospheric SO_2 concentrations greater than the equilibrium values in the figure, the forward direction of (R1) is thermodynamically preferred. Ambient SO_2 concentrations can exceed the equilibrium values, and so this reaction could occur in the atmosphere, e.g., when dust layers mix with urban pollution. Note, however, that Mg^{2+} carbonates are generally present in dust in smaller amounts than Ca^{2+} carbonates.

Kohler curves for particles with a 0.79 μm quartz core coated with highly soluble substances are shown in Figure 4. The quartz core was assumed to have been originally coated with $CaCO_3$, $MgCO_3$, or $K_2CO_3 \cdot 1.5H_2O$ to form a 0.8 μm particle. The carbonates were then converted to the corresponding nitrate, sulfite, or sulfate (as if by reaction). The dry diameters for some of the resulting particles differ slightly from 0.8 μm (see Figure 4 caption) because of the different properties of the compounds. The dramatic lowering of the saturation ratio with decreasing diameter by the presence of a small coating of highly soluble substance is evident from a comparison of the curves in Figure 4 with those for slightly soluble substances in Figure 1 and 2. Also, the results in Figure 4 indicate that differences in saturation ratios for the different HSCs are often small. This behavior suggests that the effect of the various HSCs on activation could be largely captured in cloud activation parameterizations with a single representative compound (e.g., $(NH_4)_2SO_4$).

Modified Kohler curves for particles containing 80%-quartz, 19%-$CaSO_4 \cdot 2H_2O$ or -$MgSO_3 \cdot 6H_2O$, and 1%-$Ca(NO_3)_2 \cdot 4H_2O$ or -$Mg(NO_3)_2 \cdot 6H_2O$ (mass percentages) are shown in Figure 5. The effect of the HSC on the solubility of SSC was neglected in these calculations based on the dilute nature of the solutions (Seidell and Smith, 1904). Traditional Kohler curves are also shown in Figure 5 for particles containing 99%-quartz and 1%-$Ca(NO_3)_2 \cdot 4H_2O$ or -$Mg(NO_3)_2 \cdot 6H_2O$. The slightly soluble substances lower the saturation ratios in the diameter range where the maximum occurs in the traditional curves for $Ca(NO_3)_2 \cdot 4H_2O$-SiO_2 and $Mg(NO_3)_2 \cdot 6H_2O$-SiO_2 particles. The addition of SSCs to dust particles with small amounts of HSCs could cause an initial activation stage to occur early in the cloud formation process.

3.2 Cloud Model Simulations

The maximum saturation attained in parcel simulations with externally-mixed $(NH_4)_2SO_4$ (D_g = 0.16 μm, σ_g = 1.4) and dust (D_g = 2.2 μm, σ_g = 2.0) distributions are shown as a function of updraft velocity in Figure 6. The dust particles contain 20% gypsum or 2% $Ca(NO_3)_2{\cdot}4H_2O$ by mass with the remaining mass present as a quartz core. $(NH_4)_2SO_4$ concentrations are 300 or 1000 particles cm^{-3}, and dust concentrations are 5 or 10 cm^{-3}. The $(NH_4)_2SO_4$ concentrations match values considered by Ghan et al. (1998) based on measurements in marine environments. The dust concentrations are much greater than typical atmospheric values, but airborne measurements suggest such concentrations can occur in cloud environments during large dust events (e.g., Junkermann, 2001; Levin et al., 2005). The presence of the dust distributions reduces the maximum parcel saturation because a significant amount of water vapor condenses on the dust particles (Figure 6). The absolute effect of the $Ca(NO_3)_2{\cdot}4H_2O$ distributions on maximum saturation is greater than that of the gypsum distributions, because $Ca(NO_3)_2{\cdot}4H_2O$ particles acquire water vapor throughout parcel ascent, whereas gypsum particles do not acquire water until a certain saturation is attained (see Figure 1 and 4). Gypsum distributions in turn have a greater absolute effect on maximum saturation than $CaCO_3$ distributions (curves not shown for clarity), because of the higher saturation ratios associated with $CaCO_3$ than gypsum particles. The effect of dust particles on maximum saturation is smaller for the case of 1000 $(NH_4)_2SO_4$ particles cm^{-3} than for 300 cm^{-3}—dust represents a smaller fraction of the overall surface area in the case of 1000 cm^{-3}. Similarly, the effect of coarse dust on cloud saturation is likely minor in environments where non-dust particle concentrations are >> 1000 cm^{-3}.

In Figure 7, the total number of activated particles (dust plus $(NH_4)_2SO_4$) is shown for the simulations of Figure 6. Depending on the updraft velocity, the presence of dust increases or decreases the total number of activated particles compared to the $(NH_4)_2SO_4$-only case. For an

updraft velocity of 0.05 m/s, the total number of activated particles reduces by a maximum of about 25% due to the presence of dust for $(NH_4)_2SO_4$ concentrations of 300 cm^{-3} or 1000 cm^{-3}. Competition for water vapor is significant at this low velocity, and so water uptake by dust decreases the saturation and overall number of activated particles. For an updraft velocity of 1 m/s, the total number of particles activated increases by a maximum of about 3% [$(NH_4)_2SO_4$=300 cm^{-3}] or 0.8% [$(NH_4)_2SO_4$=1000 cm^{-3}] in the presence of dust. At velocities near 1 m/s, competition for water vapor is limited, and so dust adds to the CCN population.

The total number of particles activated is shown in Figure 8 for simulations with dust distributions having D_g=1.5 μm (σ_g = 2.0) externally mixed with the standard $(NH_4)_2SO_4$ distribution. The influence of dust on the total number of activated particles is considerably less in this case compared to the one in Figure 7, where the dust D_g=2.2 μm. For $Ca(NO_3)_2{\cdot}4H_2O$-coated particles, the influence is less because of the decrease in particle surface area available for condensation associated with the decrease in mean particle size. For gypsum coated-particles, the influence is smaller because of the decrease in available surface area associated with the decrease in particle size and the corresponding increase in water vapor pressure (see gypsum-SiO_2 curves in Figure 1). The influence of composition on the activation of dust particles with different dry diameters is illustrated in Figure 9 for simulation conditions of Figure 6 and 7. The time evolution of diameter is shown for three size bins (selected from 100 bins) for $CaCO_3$, gypsum-SiO_2, and $Ca(NO_3)_2{\cdot}4H_2O$-SiO_2 dust distributions (D_g=2.2 μm, σ_g = 2.0) externally mixed with the $(NH_4)_2SO_4$ distribution (300 cm^{-3}). Parcel saturation is indicated by light grey curves. For a dry diameter of 1.1 μm ("1" curves), the $CaCO_3$ and gypsum-SiO_2 particle size does not change in time since the parcel saturation remains below the water vapor pressure. The $Ca(NO_3)_2{\cdot}4H_2O$-SiO_2 diameter grows to larger than 8 μm after 13 minutes, however, because of

the low water vapor pressure for these particles. For a diameter of 1.7 μm ("2" curves), the $CaCO_3$ size is constant, while the gypsum-SiO_2 particles activate after about 9.7 min. In this case, the gypsum-SiO_2 diameter becomes larger than the $Ca(NO_3)_2{\cdot}4H_2O$-SiO_2 diameter after about 12 min. The gypsum-SiO_2 diameter becomes larger, because the $Ca(NO_3)_2{\cdot}4H_2O$-SiO_2 particles are exposed to lower saturations due to large water consumption across the $Ca(NO_3)_2{\cdot}4H_2O$-SiO_2 size spectrum. For 2.2 μm particles ("3" curves), growth occurs for all compositions: $Ca(NO_3)_2{\cdot}4H_2O$-SiO_2 particles grow continuously, gypsum-SiO_2 particles activate after about 9.5 minutes, and $CaCO_3$ particles activate after about 9.9 minutes.

As mentioned in section 2.3, dissolution kinetics could reduce the concentration of SSC in the particle solution from the solubility value. Kinetic limitations for gypsum dissolution would increase the water vapor pressure of gypsum-coated particles and reduce the effect of these particles of on cloud properties. With dissolution rate approximated by a constant value (1.5×10^{-8} mol cm^{-2} s^{-1}, Barton and Wilde, 1971) and surface area approximated by that of the dry particle, the ratio in (4) is < 1 (no kinetic limitation) for our simulations. The ratio estimates suggest that the assumption of instantaneous dissolution for gypsum is reasonable for our exploratory purposes. Note also that calculations of diffusion in growing cloud droplets by Asa-Awuku and Nenes (2006) indicate kinetic limitations are minor for compounds with diffusivities ~10^{-9} m^2 s^{-1}, which is the case for Ca^{2+}, HSO_4^-, and SO_4^{2-} ions (Weast et al., 1987). Moreover, the influence of gypsum on dust activation is greatest for the lowest updraft velocities, where condensation is slowest.

Curves in Figure 1 of Ghan et al. (1998) illustrating the influence of trimodal sea-salt distributions externally mixed with $(NH_4)_2SO_4$ on the total number of activated particles were recalculated here using the initial condition of RH=97% (see Figure 10 here). Equilibration of

aerosol at an RH of 97% rather than 100% slightly reduces the influence of sea salt on cloud properties. Comparison of curves in Figure 10 with those in Figure 7 reveals that the sea-salt distributions have a much greater effect on the number of activated particles via water competition than the dust distributions considered above. The sea-salt distributions consume more water vapor than the dust, because sea salt is entirely soluble and the trimodal sea-salt distributions contain more particles than the single-mode dust distributions. Levin et al. (2005) observed dust distributions with three modes at an elevation of about 500 m and high fine-dust number concentrations from the surface to altitudes > 2000 m. However, based on the Kohler curves discussed above, dust particles less than about 0.8 μm are unlikely to activate unless they contain highly soluble substances or are exposed to high supersaturations, e.g., in deep convection. Fine dust particles may have smaller carbonate content than coarse dust, but HSC could form on fine dust by condensation of H_2SO_4 and NH_3 to form $(NH_4)_2SO_4$ coatings during transport.

The total number of activated particles for simulations with the standard $(NH_4)_2SO_4$ distribution externally mixed with a trimodal dust distribution (D_{g1}=0.2 μm, D_{g2}=0.8 μm, D_{g3}=2.0 μm, $\sigma_{g1}=\sigma_{g2}=\sigma_{g3}=2.0$) are shown in Figure 11. The dust particles have a SiO_2 core coated with highly soluble substance (2% by mass). Although highly soluble material in fine dust may be more likely to exist as $(NH_4)_2SO_4$ than $Ca(NO_3)_2{\cdot}4H_2O$, we represent the HSC as $Ca(NO_3)_2{\cdot}4H_2O$ throughout the distribution since $(NH_4)_2SO_4$ and $Ca(NO_3)_2{\cdot}4H_2O$ particles have similar Kohler curves. The mean diameters for the dust modes were chosen based on observations of Levin et al. (2005) over the Mediterranean Sea under dust storm conditions. Dust concentrations observed in that study appear to be greater than those indicated in Figure 11, but few of the fine particles were observed to activate. Here we consider possible effects of such

particles on cloud properties if a large fraction of them acquired soluble content during transport. For an updraft velocity of 0.05 m/s, the presence of the trimodal dust distribution reduces the total number of particles activated by a maximum of about 34% [$(NH_4)_2SO_4$=300 cm^{-3}] or 40% [$(NH_4)_2SO_4$=1000 cm^{-3}]. The large effect of the trimodal distributions on activated number via water competition is due to the large surface area and high concentration of growing particles. For an updraft velocity of 1 m/s, the presence of the trimodal distribution increases the total number of particles that activate by a maximum of about 13% [$(NH_4)_2SO_4$=1000 cm^{-3}] or 57% [$(NH_4)_2SO_4$=300 cm^{-3}]. The large effect of dust particles on cloud properties shown in Figure 11 is unlikely to occur often in the atmosphere because of the simultaneous requirements of heavily reacted dust particles, heavy dust storm conditions, and moderate background aerosol concentrations. However, the finding that large numbers of fine dust CCN can suppress precipitation (Rosenfeld et al., 2001) suggests that such conditions may exist in some instances.

Concluding remarks

The influence of dust composition on cloud saturation and droplet activation was considered in this study. Dust components were grouped into categories as insoluble, slightly soluble, or highly soluble. Dust particles were modeled as having an insoluble quartz core coated with K^+, Mg^{2+}, or Ca^{2+} compounds. All K^+ compounds, $MgSO_4 \cdot 7H_2O$, $Mg(NO_3)_2 \cdot 6H_2O$, and $Ca(NO_3)_2 \cdot 4H_2O$ were classified as highly soluble based on their bulk solubilities (Table 1). Small amounts of highly soluble components greatly enhance the ability of fine dust particles to serve as CCN. Reactions of HNO_3 or SO_2 with magnesium or calcium carbonates can potentially increase dust solubility. The reactions involving HNO_3 are particularly effective at enhancing solubility because K^+, Mg^{2+}, and Ca^{2+} nitrates are all highly soluble. The SO_2 reaction with Mg^{2+} carbonates results in a slightly soluble magnesium sulfite product that may be

oxidized to a highly soluble sulfate, while the SO_2 reaction with $CaCO_3$ produces a nearly insoluble sulfite product that can be oxidized to slightly soluble gypsum.

The importance of dust composition to dust activation is a function of particle size. For some conditions, all dust particles with diameters greater than about 2 μm activate regardless of composition. For dust particles between roughly 0.6 and 2 μm (actual range depends on conditions), the presence of slightly soluble components can induce activation of dust particles that would not activate if entirely insoluble. For dust particles with diameters less than about 0.6 μm, highly soluble substances are generally required (except under highly supersaturated conditions, e.g., deep convection) for activation to occur. Since fine dust particles may contain less carbonate than coarse dust, the heterogeneous reactions involving carbonates that can enhance dust hygroscopicity may not occur as readily in the critical fine size range. Instead, soluble content can be produced in fine dust by condensation of H_2SO_4 or may be present at emission. Considering the large concentrations of fine particles in dust storms, estimates of the small amounts of soluble material and carbonates in freshly emitted fine dust would be useful. A greater understanding of the regional prevalence of the potassium compounds and halite measured in dust by Ro et al. , Okada and Kai (2004), and others could improve estimates of water uptake by dust.

Adiabatic parcel simulations with externally-mixed $(NH_4)_2SO_4$ and coarse dust distributions were performed to understand the influence of dust on clouds via water competition. For very specialized conditions (low updraft velocity, high concentration of reacted dust, and moderate background particle concentration), coarse dust particles can significantly reduce parcel saturation and number of activated particles. However, coarse dust particles alone generally do not influence cloud properties significantly via water competition. Note that this

result does not imply that the activation of large dust particles is unimportant, since small numbers of giant dust CCN can possibly induce precipitation events and modeling the lifetime of airborne dust particles requires consideration of their potential to activate. Simulations involving trimodal dust distributions indicate that under some conditions (dust storm concentrations, heavily reacted particles, low background concentrations, and updraft velocity > ~0.5 m/s) fine dust particles can greatly enhance the number of activated particles. While the conditions necessary for this effect are not common, the previous finding that large concentrations of fine dust particles can suppress precipitation suggests that the conditions may sometimes occur.

Similarities among Kohler curves for dust containing various highly soluble compounds suggest that these components can be modeled by a single representative substance for most purposes. Also, global aerosol models could benefit by incorporating the dependence of carbonate content on dust source region and particle size, since carbonate content strongly influences dust's water uptake properties. For instance, condensation of H_2SO_4 onto a particle coated with $CaCO_3$ will likely form slightly soluble gypsum until the carbonate is depleted; further H_2SO_4 condensation leads to highly soluble content. Moreover, modeling studies indicate that heterogeneous reactions preferentially occur on fine dust because of the large surface area and long atmospheric lifetime of this mode (Bauer and Koch, 2005). However, in regions where carbonates reside primarily in the coarse mode, some reactions could preferentially occur on coarse dust. Improved representations of dust mineralogy and reactions in global aerosol models could improve predictions of the effects of aerosol on climate.

Acknowledgements

The authors thank Prof. Nicole Riemer of SUNY-Stony Brook for providing a preliminary version of the parcel model. Support for this research was provided by LLNL's Student Employee Graduate Research Fellowship (SEGRF) program and the Office of Biological and Environmental Research of the U.S. Department of Energy as part of the Atmospheric Radiation Measurement (ARM) program. This work was performed under the auspices of the U.S. Department of Energy by the University of California, Lawrence Livermore National Laboratory under contract No. W-7405-Eng-48.

References

Alpert, P., Ganor, E., 2001. Sahara mineral dust measurements from TOMS: Comparison to surface observations over the Middle East for the extreme dust storm, March 14-17, 1998. Journal of Geophysical Research-Atmospheres 106 (D16), 18275-18286.

Andronova, A.V., Gomes, L., Smirnov, V.V., Ivanov, A.V., Shukurova, L.M., 1993. Physicochemical characteristics of dust aerosols deposited during the Soviet-American Experiment (Tajikistan, 1989). Atmospheric Environment Part A-General Topics 27 (16), 2487-2493.

Asa-Awuku, A., Nenes, A., 2006. The effect of solute dissolution kinetics on cloud droplet formation: 1. Extended Kohler theory. Journal of Geophysical Research-Atmospheres [in press].

Barton, A.F.M., Wilde, N.M., 1971. Dissolution rates of polycrystalline samples of gypsum and orthorhombic forms of calcium sulphate by a rotating disc method. Transactions of the Faraday Society 65, 3590-3597.

Bauer, S.E., Koch, D., 2005. Impact of heterogeneous sulfate formation at mineral dust surfaces on aerosol loads and radiative forcing in the Goddard Institute for Space Studies general circulation model. Journal of Geophysical Research-Atmospheres 110, D17202, doi: 10.1029/2005JD005870.

Chiarello, R.P., Wogelius, R.A., Sturchio, N.C., 1993. In-situ synchrotron x-ray reflectivity measurements at the calcite-water interface. Geochimica et Cosmochimica Acta 57 (16), 4103-4110.

Dusek, U., Frank, G.P., Hildebrandt, L., Curtius, J., Schneider, J., Walter, S., Chand, D., Drewnick, F., Hings, S., Jung, D., Borrmann, S., Andreae, M.O., 2006. Size matters more than chemistry for cloud-nucleating ability of aerosol particles. Science 312 (5778), 1375-1378.

Fan, S.M., Horowitz, L.W., Levy, H., Moxim, W.J., 2004. Impact of air pollution on wet deposition of mineral dust aerosols. Geophysical Research Letters 31, L02104, doi:10.1029/2003GL018501.

Fan, S.M., Moxim, W.J., Levy, H., 2005. Implications of droplet nucleation to mineral dust aerosol deposition and transport. Geophysical Research Letters 32, L10805, doi:10.1029/2005GL022833.

Frear, G.L., Johnston, J., 1929. The solubility of calcium carbonate (calcite) in certain aqueous solutions at 25C. Journal of the American Chemical Society 51 (7), 2082-2093.

Frinak, E.K., Mashburn, C.D., Tolbert, M.A., Toon, O.B., 2005. Infrared characterization of water uptake by low-temperature Na-montmorillonite: Implications for Earth and Mars.

Journal of Geophysical Research-Atmospheres 110, D09308, doi:10.1029/2004JD005647.

Ghan, S.J., Guzman, G., Abdul-Razzak, H., 1998. Competition between sea salt and sulfate particles as cloud condensation nuclei. Journal of the Atmospheric Sciences 55 (22), 3340-3347.

Gill, T.E., 1996. Eolian sediments generated by anthropogenic disturbance of playas: Human impacts on the geomorphic system and geomorphic impacts on the human system. Geomorphology 17 (1-3), 207-228.

Goldberg, R.N., 1981. Evaluated activity and osmotic coefficients for aqueous-solutions - 36 uni-bivalent electrolytes. Journal of Physical and Chemical Reference Data 10 (3), 671-764.

Gustafsson, R.J., Orlov, A., Badger, C.L., Griffiths, P.T., Cox, R.A., Lambert, R.M., 2005. A comprehensive evaluation of water uptake on atmospherically relevant mineral surfaces: DRIFT spectroscopy, thermogravimetric analysis and aerosol growth measurements. Atmospheric Chemistry and Physics 5, 3415-3421.

Hensen, E.J.M., Smit, B., 2002. Why clays swell. Journal of Physical Chemistry B 106 (49), 12664-12667.

Junkermann, W., 2001. An ultralight aircraft as platform for research in the lower troposphere: System performance and first results from radiation transfer studies in stratiform aerosol layers and broken cloud conditions. Journal of Atmospheric and Oceanic Technology 18 (6), 934-946.

Kelly, J.T., Wexler, A.S., 2005. Thermodynamics of carbonates and hydrates related to heterogeneous reactions involving mineral aerosol. Journal of Geophysical Research-Atmospheres 110, D11201, doi:10.1029/2004JD005583.

Kline, W.D., 1929. The solubility of magnesium carbonate (nesquehonite) in water at 25 C and pressures of carbon dioxide up to one atmosphere. Journal of the American Chemical Society 51 (7), 2093-2097.

Laaksonen, A., Korhonen, P., Kulmala, M., Charlson, R.J., 1998. Modification of the Kohler equation to include soluble trace gases and slightly soluble substances. Journal of the Atmospheric Sciences 55 (5), 853-862.

Laskin, A., Wietsma, T.W., Krueger, B.J., Grassian, V.H., 2005. Heterogeneous chemistry of individual mineral dust particles with nitric acid: A combined CCSEM/EDX, ESEM, and ICP-MS study. Journal of Geophysical Research-Atmospheres 110, D10208, doi:10.1029/2004JD005206.

Levin, Z., Teller, A., Ganor, E., Yin, Y., 2005. On the interactions of mineral dust, sea-salt particles, and clouds: A measurement and modeling study from the Mediterranean Israeli Dust Experiment campaign. Journal of Geophysical Research-Atmospheres 110, D20202, doi:10.1029/2005JD005810.

Linke, W.F., Seidell, A., 1965. Solubilities, Inorganic and Metal-Organic Compounds. 4th ed. Vol. 2. American Chemical Society, Washington D.C.

Majeed, M.A., Wexler, A.S., 2001. Microphysics of aqueous droplets in clouds and fogs as applied to PM-fine modeling. Atmospheric Environment 35 (9), 1639-1653.

Masson, M.R., Lutz, H.D., Engelen, B., 1986. IUPAC Solubility Data Series: Sulfites, Selenites, and Tellurites. Vol. 26. Pergamon Press, New York.

McTainsh, G.H., Nickling, W.G., Lynch, A.W., 1997. Dust deposition and particle size in Mali, West Africa. Catena 29 (3-4), 307-322.

Meskhidze, N., Chameides, W.L., Nenes, A., 2005. Dust and pollution: A recipe for enhanced ocean fertilization? Journal of Geophysical Research-Atmospheres 110, D03301, doi:10.1029/2004JD005082.

Nenes, A., Ghan, S., Abdul-Razzak, H., Chuang, P.Y., Seinfeld, J.H., 2001. Kinetic limitations on cloud droplet formation and impact on cloud albedo. Tellus Series B-Chemical and Physical Meteorology 53 (2), 133-149.

O'Brian, F.E.M., 1948. The control of humidity by saturated salt solutions. Journal of Scientific Instruments 25, 73-76.

Okada, K., Kai, K., 2004. Atmospheric mineral particles collected at Qira in the Taklamakan desert, China. Atmospheric Environment 38 (40), 6927-6935.

Patterson, E.M., Gillette, D.A., 1977. Commonalities in measured size distributions for aerosols having a soil-derived component. Journal of Geophysical Research-Atmospheres 82 (15), 2074-2082.

Phinney, L.A., Lohmann, U., Leaitch, W.R., 2003. Limitations of using an equilibrium approximation in an aerosol activation parameterization. Journal of Geophysical Research-Atmospheres 108(D12), 4371, doi:10.1029/2002JD002391.

Pye, K., 1987. Aeolian Dust and Dust Deposits. Academic Press, Orlando.

Rard, J.A., Miller, D.G., 1981. Isopiestic determination of the osmotic coefficients of aqueous Na2SO4, MgSO4, and Na2SO4-MgSO4 At 25 C. Journal of Chemical and Engineering Data 26 (1), 33-38.

Rengemo, T., Brune, U., Sillen, L.G., 1958. Some solution equilibria involving calcium sulfite and carbonate. Acta Chemica Scandinavica 12, 873-877.

Ro, C.U., Hwang, H., Chun, Y., Van Grieken, R., 2005. Single-particle characterization of four "Asian Dust" samples collected in Korea, using low-Z particle electron probe X-ray microanalysis. Environmental Science & Technology 39 (6), 1409-1419.

Roberts, G., Mauger, G., Hadley, O., Ramanathan, V., 2006. North American and Asian aerosols over the eastern Pacific Ocean and their role in regulating cloud condensation nuclei. Journal of Geophysical Research 111, D13205, doi:10.1029/2005JD006661.

Robinson, R.A., Stokes, R.H., 1968. Electrolyte Solutions. 2nd (Revised) ed. Butterworths, London.

Rosenfeld, D., Rudich, Y., Lahav, R., 2001. Desert dust suppressing precipitation: A possible desertification feedback loop. Proceedings of the National Academy of Sciences of the United States of America 98 (11), 5975-5980.

Sarbar, M., Covington, A.K., Nuttall, R.L., Goldberg, R.N., 1982. Activity and osmotic coefficients of aqueous potassium carbonate. Journal of Chemical Thermodynamics 14 (7), 695-702.

Seidell, A., Smith, J.G., 1904. The solubility of calcium sulphate in solutions of nitrates. Journal of Physical Chemistry 8 (7), 493-499.

Seinfeld, J.H., Pandis, S.N., 1998. Atmospheric Chemistry and Physics: From Air Pollution to Climate Change. John Wiley & Sons, Inc., New York.

Seisel, S., Pashkova, A., Lian, Y., Zellner, R., 2005. Water uptake on mineral dust and soot: A fundamental view of the hydrophilicity of atmospheric particles? Faraday Discussions 130, 437-451.

Shulman, M.L., Jacobson, M.C., Charlson, R.J., Synovec, R.E., Young, T.E., 1996. Dissolution behavior and surface tension effects of organic compounds in nucleating cloud droplets. Geophysical Research Letters 23 (3), 277-280.

Singer, A., Dultz, S., Argaman, E., 2004. Properties of the non-soluble fractions of suspended dust over the Dead Sea. Atmospheric Environment 38 (12), 1745-1753.

Usher, C.R., Al-Hosney, H., Carlos-Cuellar, S., Grassian, V.H., 2002. A laboratory study of the heterogeneous uptake and oxidation of sulfur dioxide on mineral dust particles. Journal Of Geophysical Research-Atmospheres 107 (D23), Art. No. 4713.

Usher, C.R., Michel, A.E., Grassian, V.H., 2003. Reactions on mineral dust. Chemical Reviews 103 (12), 4883-4939.

Wagman, D.D., Evans, W.H., Parker, V.B., Schumm, R.H., Halow, I., Bailey, S.M., Churney, K.L., Nuttall, R.L., 1982. The NBS tables of chemical thermodynamic properties - selected values for inorganic and C-1 and C-2 organic substances in Si units. Journal of Physical and Chemical Reference Data 11, 1-&.

Wang, Y.Q., Zhang, X.Y., Arimoto, R., Cao, J.J., Shen, Z.X., 2005. Characteristics of carbonate content and carbon and oxygen isotopic composition of northern China soil and dust aerosol and its application to tracing dust sources. Atmospheric Environment 39 (14), 2631-2642.

Weast, R.C., Astle, M.J., Beyer, W.H., 1987. CRC Handbook of Chemistry and Physics, 67th Edition. CRC Press, Boca Raton, Florida.

Wells, R.C., 1915. The solubility of magnesium carbonate in natural waters. Journal of the American Chemical Society 37 (7), 1704-1707.

Wurzler, S., Reisin, T.G., Levin, Z., 2000. Modification of mineral dust particles by cloud processing and subsequent effects on drop size distributions. Journal of Geophysical Research-Atmospheres 105 (D4), 4501-4512.

Yin, Y., Wurzler, S., Levin, Z., Reisin, T.G., 2002. Interactions of mineral dust particles and clouds: Effects on precipitation and cloud optical properties. Journal of Geophysical Research-Atmospheres 107 (D23), Art. No. 4724, doi: 4710.1029/2001JD001544.

Figure Legends

Figure 1. Kohler curves for particles (dry diameter = 0.8 μm) having a SiO_2 (quartz) core coated with slightly soluble calcium compounds. Mass percentages of calcium compound are indicated with the remaining mass as a SiO_2 core. 'gyp' indicates gypsum ($CaSO_4 \cdot 2H_2O$).

Figure 2. Kohler curves for particles (dry diameter = 0.8 μm) having a SiO_2 (quartz) core coated with slightly soluble magnesium compounds. Mass percentages of magnesium compound are indicated with the remaining mass as a SiO_2 particle core. 'MC' indicates $MgCO_3 \cdot 3H_2O$ and 'MS' indicates $MgSO_3 \cdot 6H_2O$.

Figure 3. Equilibrium concentrations of $SO_2(g)$ for reaction (R1) with hydration number n = 3 or 6. CO_2 concentration = 350 ppm, T=298 K, P=1000 mbar. Thermodynamic properties from Wagman et al. (1982); calculations according to Kelly and Wexler (2005). Curves indicate the forward direction of (R1) is preferred for some atmospheric conditions (when $[SO_2]_{ambient} > [SO_2]_{Equilibrium}$). Note: curves indicate that $MgSO_3 \cdot 3H_2O(s)$ is stable even for RH near 100%, where $MgSO_3 \cdot 6H_2O(s)$ is known to be the stable phase for T < 313 K (Masson et al., 1986). This discrepancy could result from small inaccuracies in thermodynamic properties.

Figure 4. Kohler curves for particles having a 0.79 μm SiO_2 core coated with highly soluble compounds. Dry diameters for particles with different coatings as follows: $(NH_4)_2SO_4$, $K_2CO_3 \cdot 1.5H_2O$, K_2SO_4, and K_2SO_3 = 0.8 μm; $Ca(NO_3)_2 \cdot 4H_2O$ = 0.82 μm; $Mg(NO_3)_2 \cdot 6H_2O$ and $MgSO_4 \cdot 7H_2O$ = 0.84 μm.

Figure 5. Kohler curves for particles (dry diameter = 0.8 μm) having an insoluble quartz core coated with slightly soluble and highly soluble substances. Compositions as follows (mass percentages): 1% $Mg(NO_3)_2 \cdot 6H_2O$-99% SiO_2; 1% $Ca(NO_3)_2 \cdot 4H_2O$-99% SiO_2; 1% $Ca(NO_3)_2 \cdot 4H_2O$-19% gypsum-80% SiO_2; 1% $Mg(NO_3)_2 \cdot 6H_2O$-19% $MgSO_3.6H_2O$-80% SiO_2.

Figure 6. Maximum saturation ratio as a function of updraft velocity for adiabatic parcel simulations having a lognormal $(NH_4)_2SO_4$ distribution (D_g=0.16 μm, σ_g=1.4) externally mixed with a lognormal dust distribution (D_g=2.2 μm, σ_g=2.0). Mass percentages of coatings are indicated for dust distributions with the remaining mass as a SiO_2 particle core. Total particle number concentrations are indicated for each distribution.

Figure 7. Total number of particles [$(NH_4)_2SO_4$ plus dust] that activate for simulations of Figure 6.

Figure 8. Same as Figure 7, except dust distribution has D_g=1.5 μm rather than D_g=2.2 μm.

Figure 9. Time evolution of particle diameter and water saturation for parcel simulations of Figure 6 [$(NH_4)_2SO_4$ = 300 cm^{-3}]. Differences in growth occur for particles with the same dry diameter (Ddry) but with insoluble ($CaCO_3$), slightly soluble (gypsum), or highly soluble ($Ca(NO_3)_2.4H_2O$) components. 'CN' indicates saturation curve corresponding to simulation with dust particles coated by $Ca(NO_3)_2.4H_2O$ (2% by mass).

Figure 10. Total number of particles [$(NH_4)_2SO_4$ plus sea salt] that activate for simulations described in Figure 1 of Ghan et al. (1998). Curves shown here are for initial equilibration of aerosol at RH of 97% rather than 100%. U-values correspond to wind speeds that result in the trimodal distributions described by Ghan et al. (1998) (e.g., D_{g1}=0.2 μm, D_{g2}=2 μm, D_{g3}=12 μm).

Figure 11. Total number of particles [$(NH_4)_2SO_4$ plus dust] that activate as a function of updraft velocity for simulations with an $(NH_4)_2SO_4$ distribution (D_g=0.16 μm, σ_g=1.4) externally mixed with a trimodal dust distribution containing 2% $Ca(NO_3)_2{\cdot}4H_2O$-98% SiO_2 particles (mass percentages). Trimodal dust parameters are as follows: D_{g1}=0.2 μm, D_{g2}=0.8 μm, D_{g3}=2 μm, $\sigma_{g1}=\sigma_{g2}=\sigma_{g3}$=2.0 (total number concentrations for modes are given in figure).

Table 1. Saturation properties of dust components at 298 K (unless noted otherwise)

Dust Components	DRH (%)	m_{sat} (mol kg^{-1})
$Ca(NO_3)_2{\cdot}4H_2O$	50.0[a]	8.41[f]
$CaSO_4{\cdot}2H_2O$	–[j]	1.5×10^{-2} [e]
$CaSO_3{\cdot}0.5H_2O$	~100[i]	7.6×10^{-4} [e]
$CaCO_3$	~100[i]	5.3×10^{-4} [g]
$Mg(NO_3)_2{\cdot}6H_2O$	52.9[a]	4.90[f]
$MgSO_4{\cdot}7H_2O$	90.4[c]	3.0211[c]
$MgSO_3{\cdot}6H_2O$	–	5.0×10^{-2} [h]
$MgCO_3{\cdot}3H_2O$	–	1.5×10^{-2} [k]
$MgCO_3$	~100[i]	8.2×10^{-4} [k]
$K_2CO_3{\cdot}1.5H_2O$	44.5[b]	8.102[b]
K_2SO_3	–	6.07[f]
KNO_3	92.5[a]	3.75[f]
K_2SO_4	97.5[d]	0.692[d]
$(NH_4)_2SO_4$	80.0[a]	5.78[f]

Symbols: DRH = deliquescence relative humidity, m_{sat} = saturation molality
[a]Robinson and Stokes (1968)
[b]Sarbar et al. (1982)
[c]Rard and Miller (1981)
[d]Goldberg (1981)
[e]Rengemo et al. (1958)
[f]Linke and Seidell (1965)
[g]Frear and Johnston (1929)
[h]Masson et al. (1986)
[i]Based on low solubility
[j]O'Brien (1948) gives 98% for $CaSO_4{\cdot}5H_2O$
[k]Wells (1915) T=293 K

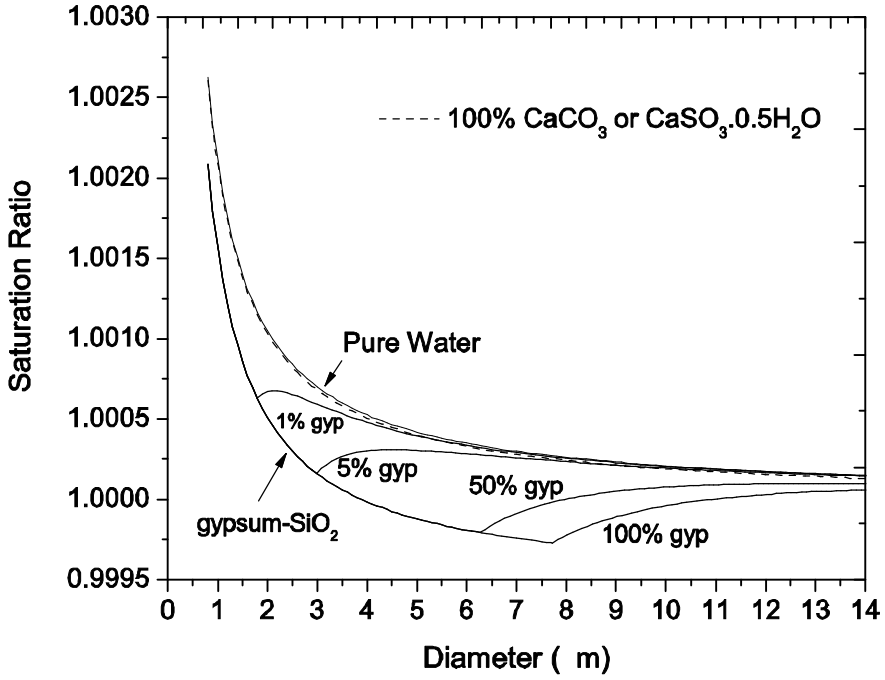
1.0030
1.0025
1.0020
1.0015
1.0010
1.0005
1.0000
0.9995
Saturation Ratio
0 1 2 3 4 5 6 7 8 9 10 11 12 13 14
Diameter (m)
100% CaCO3 or CaSO3.0.5H2O
Pure Water
1% gyp
5% gyp
50% gyp
100% gyp
gypsum-SiO2

Figure 1

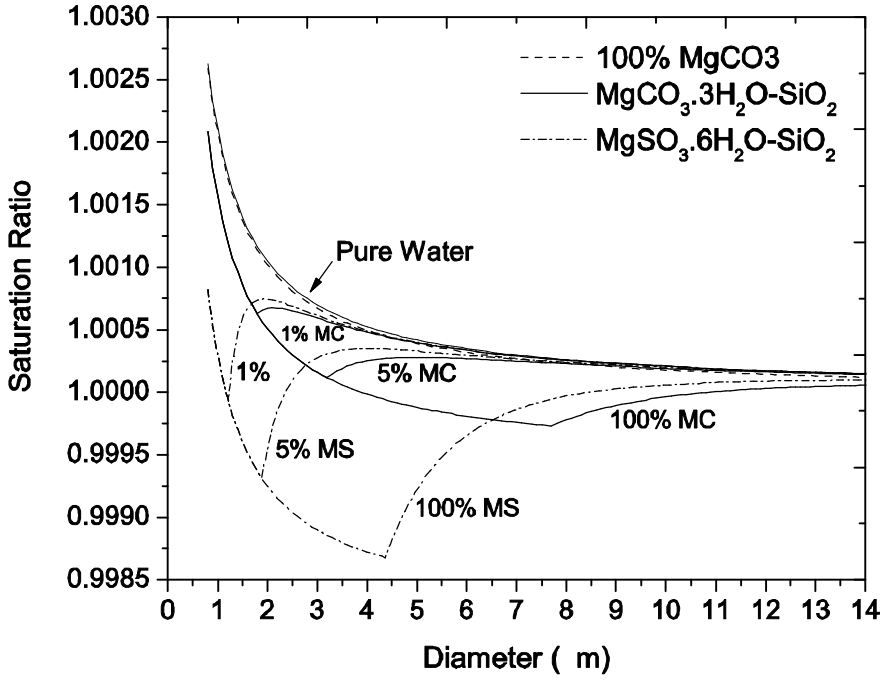
100% MgCO3
MgCO3.3H2O-SiO2
MgSO3.6H2O-SiO2
Pure Water
1% MC
1%
5% MC
100% MC
5% MS
100% MS
Saturation Ratio
Diameter (m)
1.0030
1.0025
1.0020
1.0015
1.0010
1.0005
1.0000
0.9995
0.9990
0.9985
0 1 2 3 4 5 6 7 8 9 10 11 12 13 14

Figure 2

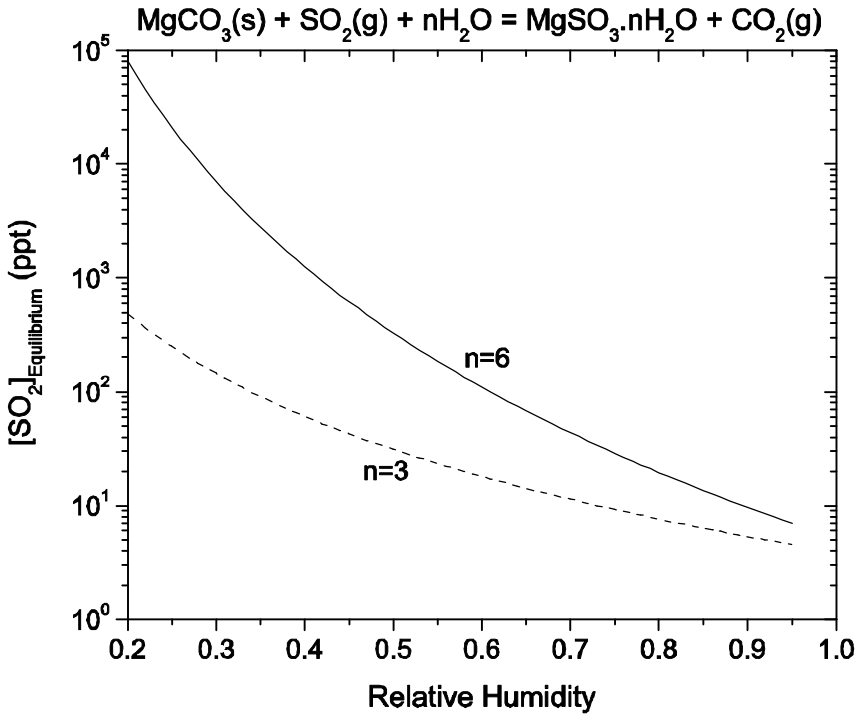
MgCO3(s) + SO2(g) + nH2O = MgSO3.nH2O + CO2(g)
[SO2]Equilibrium (ppt)
Relative Humidity
n=6
n=3
10^5
10^4
10^3
10^2
10^1
10^0
0.2
0.3
0.4
0.5
0.6
0.7
0.8
0.9
1.0

Figure 3

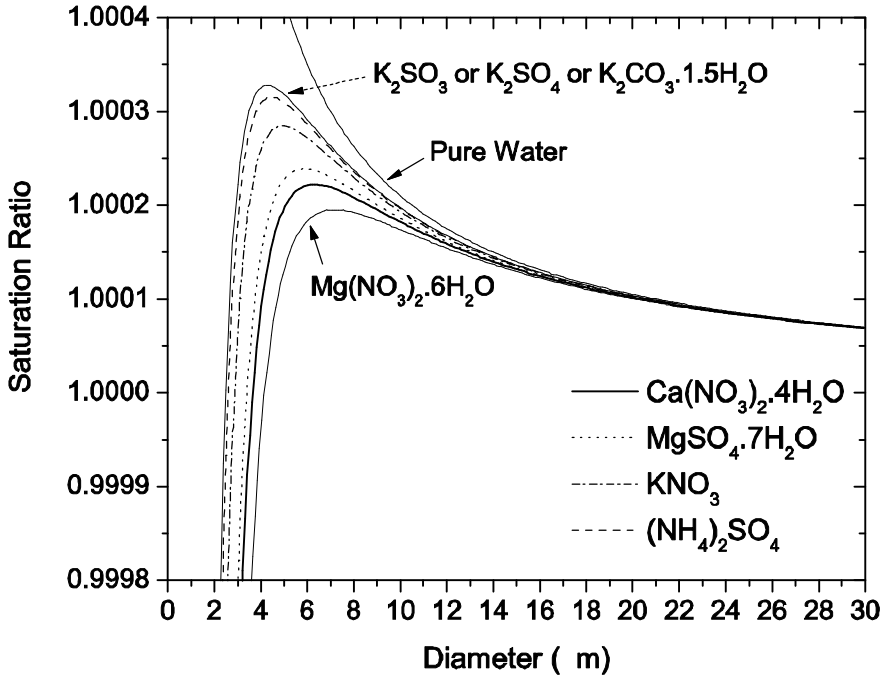
1.0004
1.0003
1.0002
1.0001
1.0000
0.9999
0.9998
Saturation Ratio
0 2 4 6 8 10 12 14 16 18 20 22 24 26 28 30
Diameter (m)
K2SO3 or K2SO4 or K2CO3.1.5H2O
Pure Water
Mg(NO3)2.6H2O
Ca(NO3)2.4H2O
MgSO4.7H2O
KNO3
(NH4)2SO4

Figure 4

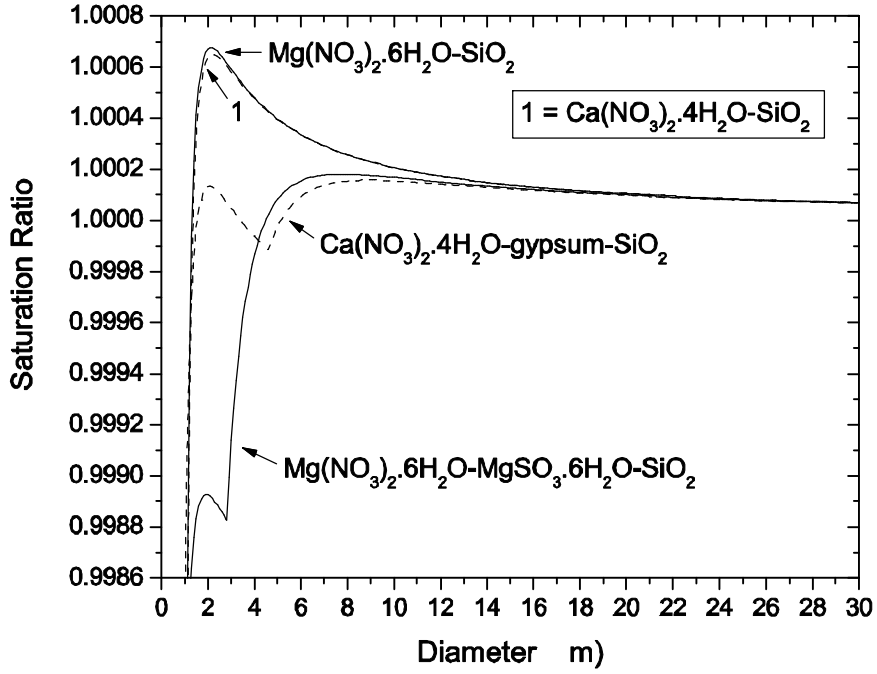
Saturation Ratio
Diameter m)
Mg(NO3)2.6H2O-SiO2
1
1 = Ca(NO3)2.4H2O-SiO2
Ca(NO3)2.4H2O-gypsum-SiO2
Mg(NO3)2.6H2O-MgSO3.6H2O-SiO2
1.0008
1.0006
1.0004
1.0002
1.0000
0.9998
0.9996
0.9994
0.9992
0.9990
0.9988
0.9986
0 2 4 6 8 10 12 14 16 18 20 22 24 26 28 30

Figure 5

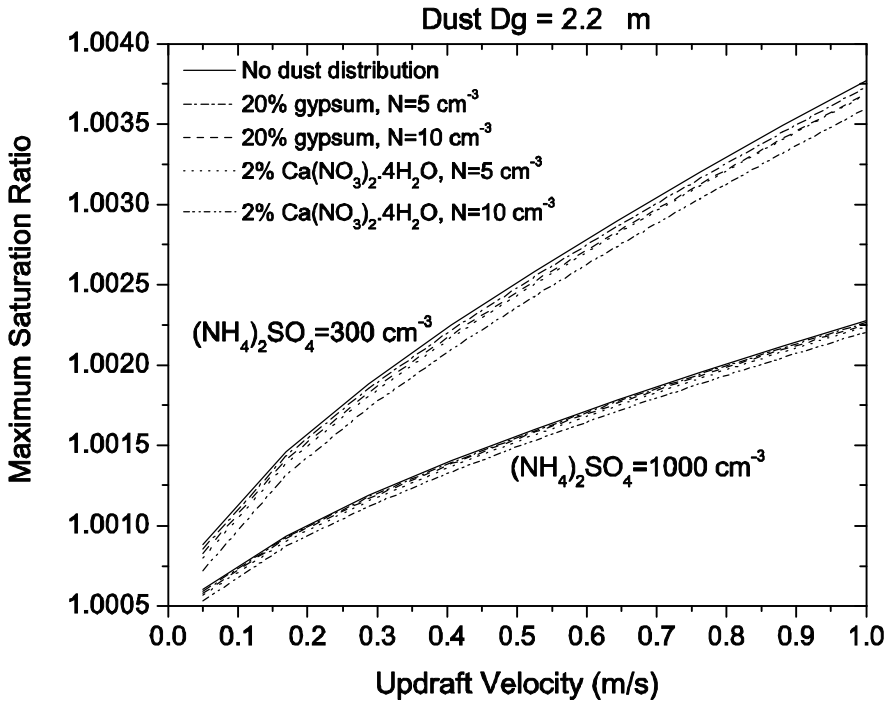
Dust Dg = 2.2 m
Maximum Saturation Ratio
Updraft Velocity (m/s)
No dust distribution
20% gypsum, N=5 cm-3
20% gypsum, N=10 cm-3
2% Ca(NO3)2.4H2O, N=5 cm-3
2% Ca(NO3)2.4H2O, N=10 cm-3
(NH4)2SO4=300 cm-3
(NH4)2SO4=1000 cm-3
1.0040
1.0035
1.0030
1.0025
1.0020
1.0015
1.0010
1.0005
0.0
0.1
0.2
0.3
0.4
0.5
0.6
0.7
0.8
0.9
1.0

Figure 6

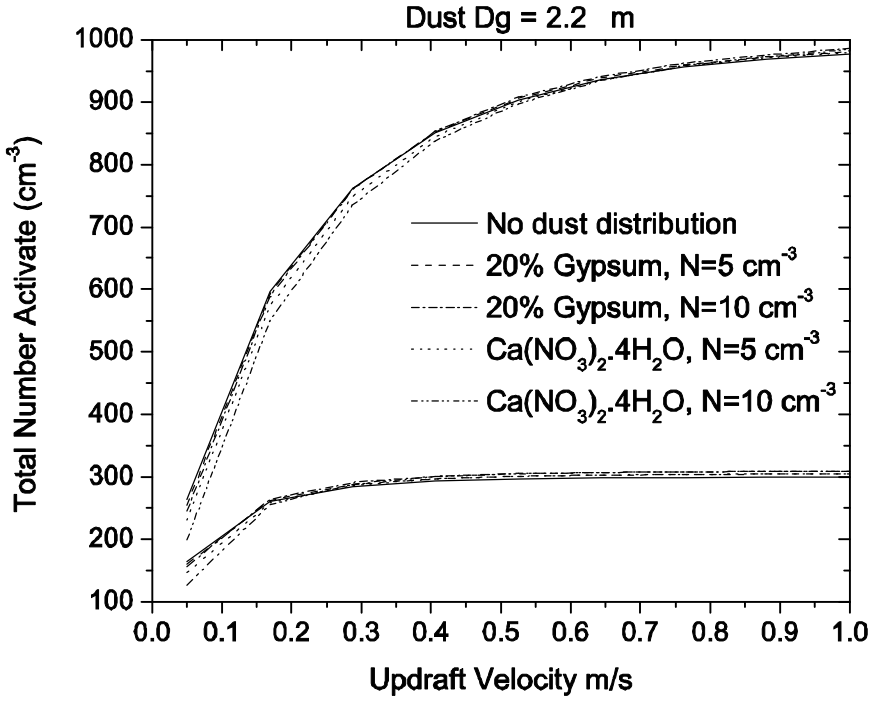
Dust Dg = 2.2 m
Total Number Activate (cm-3)
Updraft Velocity m/s
No dust distribution
20% Gypsum, N=5 cm-3
20% Gypsum, N=10 cm-3
Ca(NO3)2.4H2O, N=5 cm-3
Ca(NO3)2.4H2O, N=10 cm-3
1000
900
800
700
600
500
400
300
200
100
0.0
0.1
0.2
0.3
0.4
0.5
0.6
0.7
0.8
0.9
1.0

Figure 7

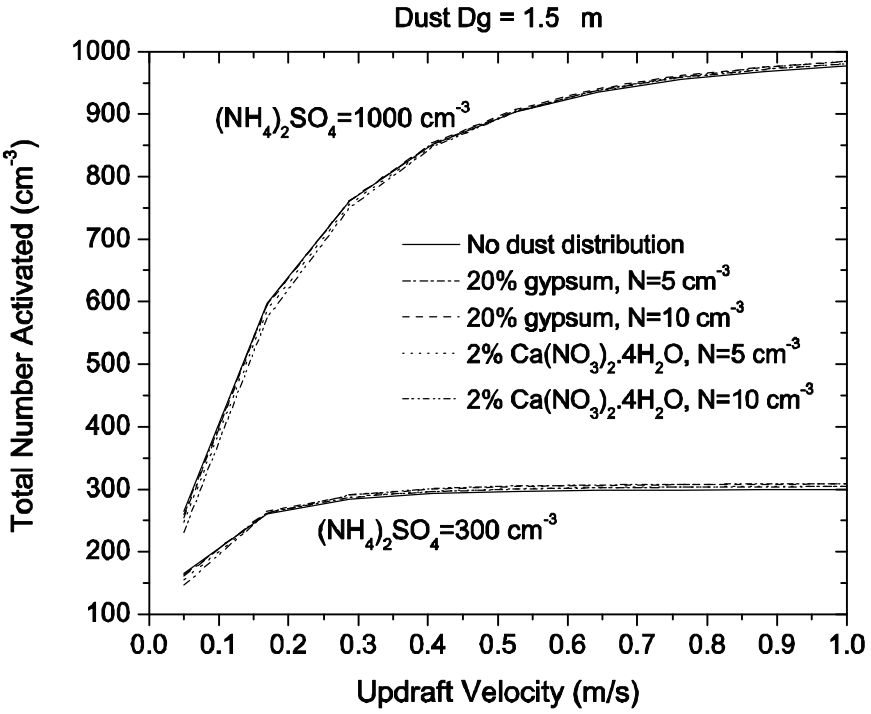
Dust Dg = 1.5 m
Total Number Activated (cm-3)
Updraft Velocity (m/s)
(NH4)2SO4=1000 cm-3
(NH4)2SO4=300 cm-3
No dust distribution
20% gypsum, N=5 cm-3
20% gypsum, N=10 cm-3
2% Ca(NO3)2.4H2O, N=5 cm-3
2% Ca(NO3)2.4H2O, N=10 cm-3
1000
900
800
700
600
500
400
300
200
100
0.0
0.1
0.2
0.3
0.4
0.5
0.6
0.7
0.8
0.9
1.0

Figure 8

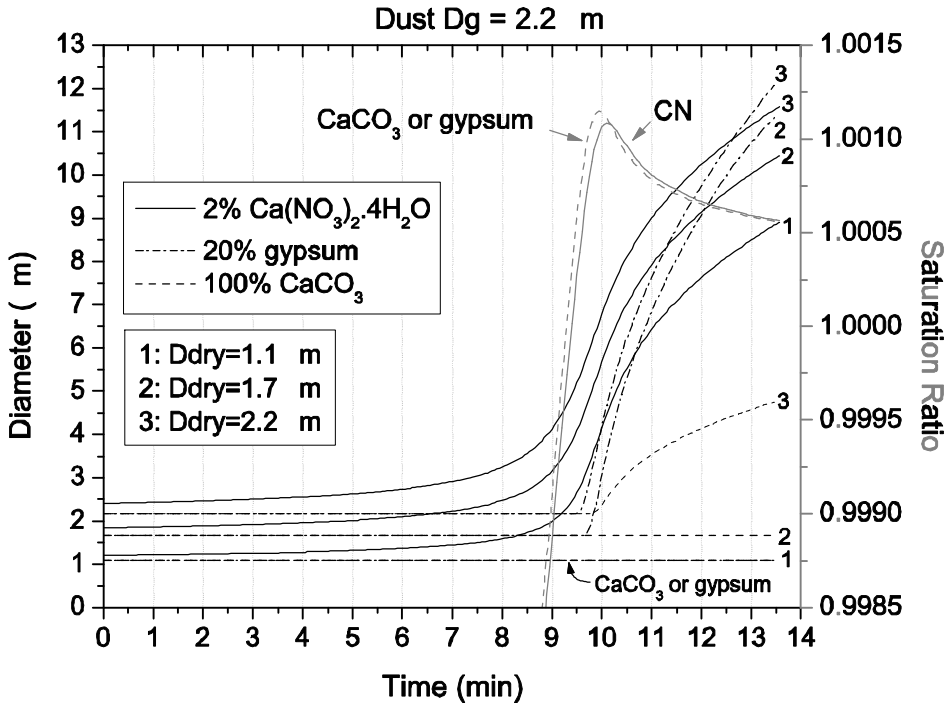
Dust Dg = 2.2 m
Diameter (m)
Saturation Ratio
Time (min)
CaCO3 or gypsum
CN
2% Ca(NO3)2.4H2O
20% gypsum
100% CaCO3
1: Ddry=1.1 m
2: Ddry=1.7 m
3: Ddry=2.2 m
CaCO3 or gypsum

Figure 9

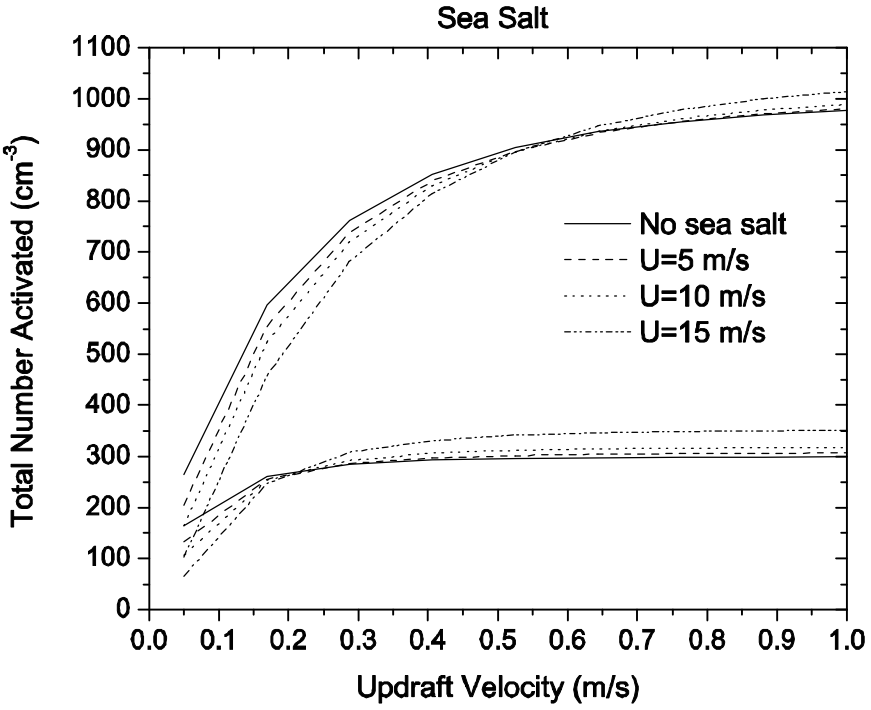
Sea Salt
Total Number Activated (cm-3)
Updraft Velocity (m/s)
No sea salt
U=5 m/s
U=10 m/s
U=15 m/s
0
100
200
300
400
500
600
700
800
900
1000
1100
0.0
0.1
0.2
0.3
0.4
0.5
0.6
0.7
0.8
0.9
1.0

Figure10

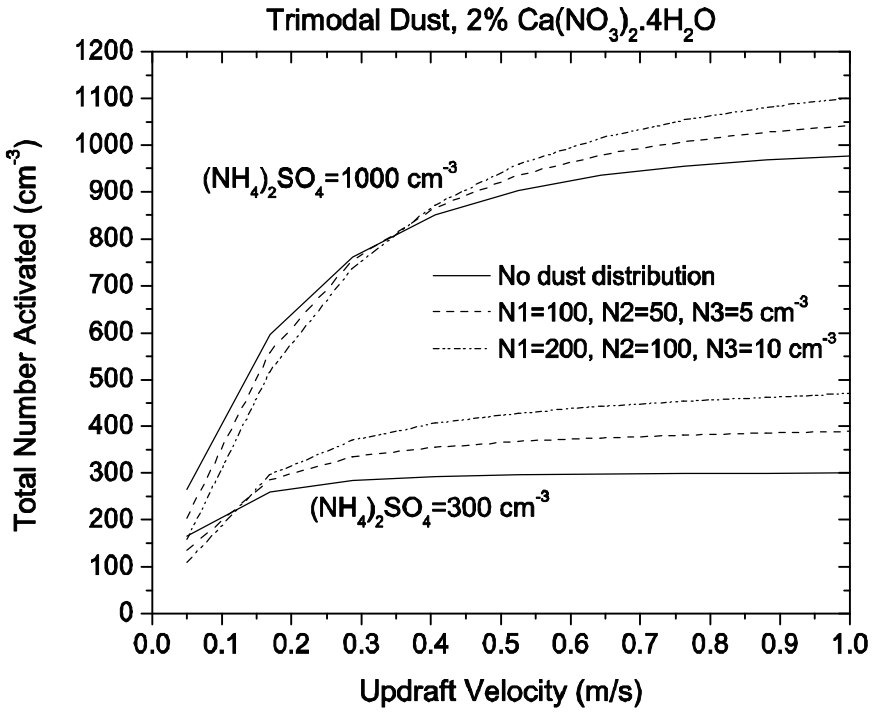
Trimodal Dust, 2% Ca(NO3)2.4H2O
Total Number Activated (cm-3)
Updraft Velocity (m/s)
(NH4)2SO4=1000 cm-3
(NH4)2SO4=300 cm-3
No dust distribution
N1=100, N2=50, N3=5 cm-3
N1=200, N2=100, N3=10 cm-3
0
100
200
300
400
500
600
700
800
900
1000
1100
1200
0.0
0.1
0.2
0.3
0.4
0.5
0.6
0.7
0.8
0.9
1.0

Figure 11